Three-Dimensional Numerical Simulation of the flow past a circular cylinder based on LES method

CHEN Hai-long, DAI Shao-shi, LI Jia，YAO Xiong-liang

College of Shipbuilding Engineering, Harbin Engineering University, Harbin 150001,China

Abstract: The hydrodynamic characteristics of rigid single circular cylinder in three dimensional incompressible uniform cross flow was calculated using Large-eddy simulation method of CFX5 in this paper. Solution to the three dimensional N-S equations were obtained by the finite volume method. The focus of numerical simulation was to research characteristics of the pressure distribution (drag and lift force.) and vortex tube at high Reynolds number. The results of calculation show that the forces of every section along spanwise of cylinder are symmetrical about the middle section and smaller than two dimensional case. Moreover the flow around the cylinder obviously presents three dimensional characteristics.

Keywords: LES method; Flow past tree dimensional circular cylinder; Hydrodynamic characteristics

Introduction

The phenomenon of Flow around a Cylinder widely exists in the engineering, especially in ocean engineering and wind engineering. This problem received widespread attention in the 60-90 age of the 20th century and a large number of studies have been published. But due to the restriction of theory, experiment condition and other facts, most of experiments were hard to carry out when Reynolds number was high. With the speed and capacity of computer increased rapidly, Simulation technology is getting more and more sophisticated; simulation research has become an effective means of turbulence research.

Right now many scholars at home and abroad have carried out in-depth research in 2-dimension flow around a cylinder. But there are few articles published about the research of 3-dimension flow around a cylinder. Wang yaling simulated 3-dimensional incompressible and viscous flow around a cylinder in finite volume method and SIMPLE calculation format （Re=1000 and Re=10000）. They found that the fluid around the cylinder had obvious 3-dimension characteristics when the Reynolds number is high. Germans M.Breuer simulated the 3-dimension flow around a cylinder in large eddy simulation (LES) (Re=14000). His research showed that 3-dimension simulations about flow around a cylinder in LES were much closed to experimental results. American Juan P.Pontaza and Hamn-Ching Chen made 3-dimension simulation about Cylindrical vortex-induced vibration that has 2 degree freedom and the simulation results were very closed to the results that Achenbach(1968) and Schewe(1983) had calculated.

This article simulated three-dimensional hydrodynamic characteristics in uniform flow around a cylinder with the method of LES in CFX5, compared with the results other scholars had simulated, validate and analyze availability and rule of numerical experiment.

1 Mathematical Model

1.1 Controlling Equation

This article adopts advanced turbulent model LES to

numerically simulate the hydrodynamic characteristics of the rigid isolated cylinder. The problem is described as Section 1.

The model LES mostly uses the method of filtering to decomposed the vortex in the wakes into a large scale one and a small scale one,and then numerically solves them and calculates and analyses them respectively. The model LES is to decompose the flow variables in the flow fields into a large scale one (solvable) and a small scale one (unsolvable, use the model SGS to simulate). For an arbitrary transient, the fluid variable f is written as: $f = \overline{f} + f'$.

The large scale variable after filtering is:

$$\bar{f}(x_i,t) = \int_{Vol} G(x_i - x_i')f(x_i',t)dx_i' \qquad (1)$$

Where, $\overline{f}$ is the large scale variable,and is defined by volume-averaged, f' is the small scale variable, and reflects the small-scale movement's contribution for f. It is also named as Sub-grid-scale Component.

$G(x_i - x_i')$----Gaussian filter.

After the continuity equation and the 3-D incompressible Navier-Stokes equation are filtered, we introduce the model SGS to write it as:

$$\nabla \cdot u = 0 \qquad (2)$$

$$\frac{\partial \rho \overline{u_i}}{\partial t} + \frac{\partial}{\partial x_j}(\rho \overline{u_i u_j}) = -\frac{\partial p}{\partial x_i} + \mu \frac{\partial^2 \overline{u_i}}{\partial x_j x_j} + \frac{\partial \tau_{ij}}{\partial x_j} \qquad (3)$$

$$\tau_{ij} = \nu_{SGS} \cdot (\frac{\partial \bar{u_i}}{\partial x_j} + \frac{\partial \bar{u_j}}{\partial x_i}) \qquad (4)$$

Where, $\overline{u}$ and $\overline{v}$ are the velocity along x-axis and the velocity along y-axis in the Cartesian coordinate system after filtering respectively, $\overline{p}$ is the pressure in the Cartesian coordinate system; τ_{ij} is the unsolved Sub-grid-scale Turbulent Stress; ν_{SGS} is the Sub-grid-scale eddy viscosity coefficient; $\nu_{SGS} \propto l q_{SGS}$, $l = \Delta = (Vol)^{1/3}$, Δ is the gird width; q_{SGS} is the unsolved velocity.

$$q_{SGS} = \Delta \left| \bar{S} \right| = \Delta \left(2 \overline{S}_{ij} \overline{S}_{ij} \right)^{1/2}$$

$$\tau_{ij} = (C_S \Delta)^2 \bar{S} \qquad (5)$$

Where C_S is the Smagorinsky Constant, this article selects $C_S = 0.1$. Equarion (4) is substituted into the equation (3) to solve the equations (2) and (3).

1.2 Initial Conditions and Boundary Conditions

In order to solve the motion equation of the viscous fluid better, we must reasonably define the initial conditions and the boundary conditions of the flow field. This article defines them as follows.

Boundary conditions of the rigid column wall surface: There is no slip at the interface between fluid and solid, that is $u_n = 0$.

The initial conditions of the unsteady viscous fluid: The reference pressure of the flow field is 1atm, and the water temperature is 15℃. The velocity of the uniform flow at infinite point of the flow field is u_∞.

The far field condition is: at infinite point of the flow field (the export of the flow field), the average static pressure $p = 0$.

1.3 The Establishment of the Model and the Grid Dividing

Reference [3] gives that when the spanwise length of the cylinder $Z \geq \pi D$, the cylinder's flow problems

will present obvious three-dimensional effect. This article made many times of debugging with reference to reference [2] and [6~9], and finally determined the dimension and the arrangement mode of the computational flow field (Fig.1).

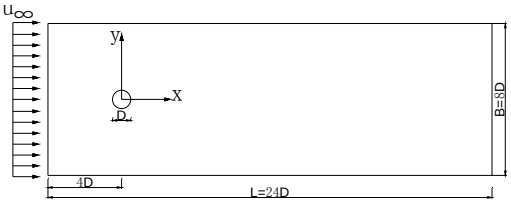

(a)

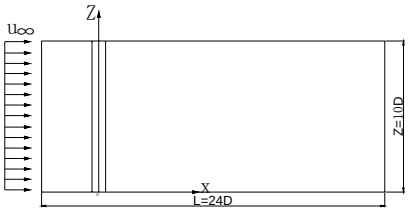

(b)

Fig.1 Arrangement of the computational flow field

This article adopts unstructured mesh (Hex8) to mesh the whole flow field. When constructing the mesh, we divide the computational domain into 9 regions. In the region near the wall of the cylinder, the mesh is dense, and in other regions, the mesh becomes sparser gradually. In this article, the number of the spanwise mesh is 50, and the number of the computational mesh is 944000.

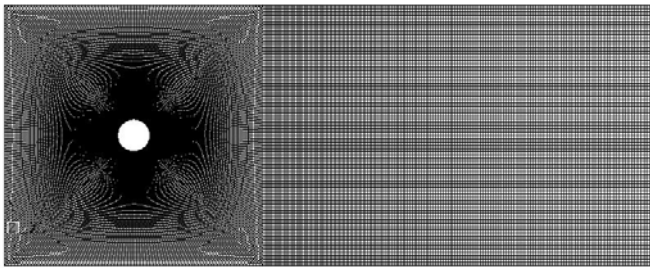

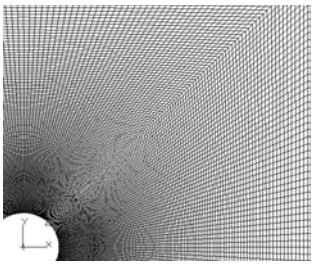

Fig. 2 Schematic diagram of the meshing plan

2 The Definition of the Dimensionless Parameters

2.1 The Stable Pressure Coefficients and The Fluctuating Pressure Coefficients

$$C_{p0}(\theta)=\frac{P_0(\theta)-P_\infty}{1/2\cdot\rho\cdot u_\infty{}^2} \tag{6}$$

$$C_p^{'}(\theta,t)=\frac{P'(\theta,t)}{1/2\cdot\rho\cdot u_\infty{}^2} \tag{7}$$

Where, $p_0(\theta)$ and $p'(\theta,t)$ are the stable pressure and the fluctuating pressure at each measuring point of the cylinder surface, respectively; p_∞, u_∞, ρ are the hydrostatic pressure, the freestream velocity and the density of the fluid at infinite point.

2.2 The Stable Lift Coefficients and Resistance Coefficients and The Fluctuating Ones at Each Section of the Cylinder.

$$C_{do}=\frac{1}{2}\int_0^{2\pi}C_{p0}(\theta)\cos\theta d\theta \tag{8}$$

$$C_{lo}=\frac{1}{2}\int_0^{2\pi}C_{p0}(\theta)\sin\theta d\theta \tag{9}$$

$$C_l^{'}(t)=\frac{1}{2}\int_0^{2\pi}C_p^{'}(\theta,t)\sin\theta d\theta \tag{10}$$

$$C_d^{'}(t)=\frac{1}{2}\int_0^{2\pi}C_p^{'}(\theta,t)\cos\theta d\theta \tag{11}$$

In this article, the fluctuating lift coefficients and the fluctuating resistance coefficients adopts the

corresponding root mean square values, that is $C_l^{'} = \sqrt{E\left[C_L^{'}(t)\right]^2}$, $C_d^{'} = \sqrt{E\left[C_d^{'}(t)\right]^2}$. The definition of θ is shown in Fig. 3(a).

2.3 The Lift Coefficients and the Resistance Coefficients of the Whole Cylinder

$$C_l(t) = \frac{F_l(t)}{1/2 \cdot \rho \cdot V^2 HD} \qquad (12)$$

$$C_d(t) = \frac{F_d(t)}{1/2 \cdot \rho \cdot V^2 HD} \qquad (13)$$

Where $F_l(t)$ and $F_d(t)$ are the lift and the resistance (N) on the whole cylinder; H are the spanwise height of the cylinder. $C_l^{'}$ and $C_d^{'}$ also adopt the root mean square values, and its algorithm is the same as above.

3 The Numerical Calculation Results and Analysis

This article layouts a pressure sensing point every 15 degrees in the circumferential direction of the cylinder, and selects 5 pressure sensing surfaces in the spanwise derection of the cylinder, and then gives a detailed analysis of the distribution law of the stable pressure coefficients and the fluctuating pressre coefficients of each pressure sensing surface (It is shown in Fig. 3(b)). In our analysis, we adopt the height from each section to the origin to difine the section.

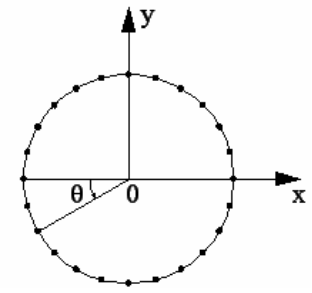

(a)

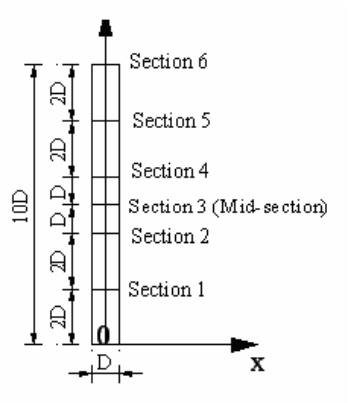

(b)

Fig.3 Schematic diagram of the pressure sensing points and surfaces of the cylinder

3.1 The Circumferential Distribution of the Stable and Fluctuating Pressure Coefficients of the Cylinder

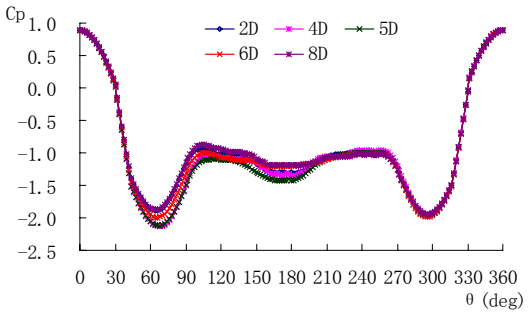

(a)

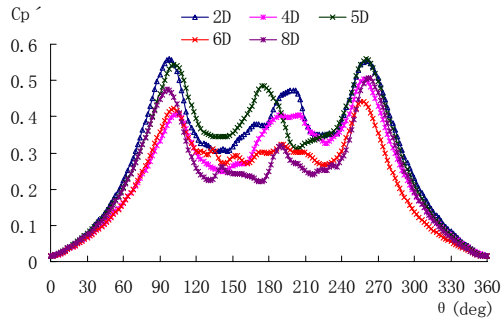

(b)

Fig.4 Circumferential distribution of the cylinder's stable pressure coefficients at each section (a) and the fluctuating pressure coefficients (b)

In Fig.4 (a) we can see that C_{p0} is the maximum at

the stagnation point of the cylinder ($\theta = 0^\circ$或360°), about 0.9. With the inflow's extension to both sides of the cylinder, C_{p0} reduces to its minimum rapidly. When $\theta = 60^\circ$ or $\theta = 300^\circ$, it is about -1.8. Its value in the back pressue rigion is about -1.0~-1.2. In Fig. 4 (b) we can see that $C_p^{'}$ is the minimum at the stagnation point of the cylinder, about 0.011. When $\theta = 90^\circ$ and $\theta = 270^\circ$, symmetric peak turns up, and then it decreases to a flat value. But on this condition, changes of fluctuating pressure coefficients at different section are not the same. Section 1's and section 2's second peaks appear when $\theta = 195^\circ$, and section 3's small peak appears when $\theta = 180^\circ$, while changes of section 4 and section 5 in this rigion are not obvious. When is the same, Reference [10] gives the two-dimensional experimental results of the flow around cylinder. The maximum of C_{p0} is 1.0 when $\theta = 0^\circ$或360°, and its minimum is about -1.6, and in the back pressure rigion C_{p0} is about -1.2. The peak of $C_p^{'}$ appears when $\theta = 75^\circ$和285°, and its minimum is about 0.1. By contrast we can see that the values of C_{p0} and $C_p^{'}$ obtained in the numerical experiment of the three-dimensional flow around cylinder are all slightly smaller than those in the two-dimensional experiment. C_{p0} at each section has no significant change, while $C_p^{'}$ changes greatly.

3.2 Abscisic Point of the Vortex and the Wake Pressure

The definition of the abscisic point and its detachment angle of the vortex are shown in Fig. 5. Changes of the vortex's separation point at each section in the spanwise direction are show in Fig. 6. At each section in the spanwise direction, we layout a measuring point every 2D from x-axis to the central point of the cylinder at that section, then each spanwise section has 10 measuring points, as shown in Fig. 5.

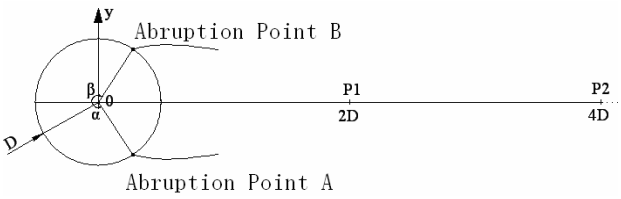

Fig. 5 Schematic diagram of the separation point and measuring points of the section

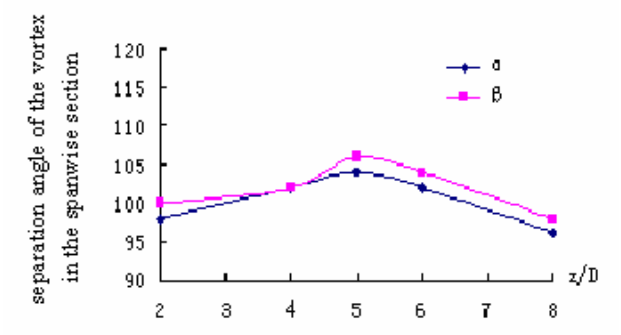

Fig. 6 changes of the separation angle of the vortex in the spanwise section

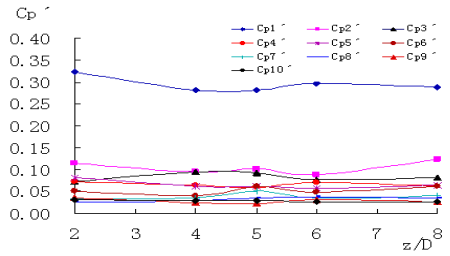

Fig. 7 changes of $C_p^{'}$ in the spanwise section

In Fig. 6 we can see that the abscisic points of the vortex at different sections are not the same. The abscisic points of the vortex at the five sections in the spanwise direction of the cylinder move to the back pressure rigion gradually from the end section to the middle section, that is the vortex's abscisic angle of the middle section are larger than that of the end section, and changes of the vortex's abscisic angles α

and β show symmetry in the spanwise direction when fluid flows around three-dimensional cylinder. This suggests that when the reynolds number and the spanwise length are as above, flowing around the cylinder shows abvious three-dimensional character.

In Fig. 7 we can see that the values of $C_p^{'}$ of points in the wake flow rigion of the cylinder at each spanwise section are larger near the wall of the cylinder, while with the increase of the distance, the values of $C_p^{'}$ markedly decrease to about zero and show smooth changes. Meanwhile, the values of $C_p^{'}$ of the measuring points near the wall change obviously, and they change very smoothly in the spanwise direction far away form the wall of the cylinder. This suggests that the three-dimensional character of the pressure near the wall of the cylinder is stronger than that far away from the wall. The value of $C_p^{'}$ shows obvious two-dimensional character far away fron the wall of the cylinder, namely after $x = 16D$.

3.3 The Spanwise Distribution of the Lift Coefficients and the Resistance Coefficients at Each Section of the Cylinder

The duration curves of the lift coefficients and the resistance coefficients in the spanwise direction at each section of the cylinder are shown in Fig. 8. C_{l1} and C_{l2} respectively represent the lift coefficients of section 1 and section 2, and the others are in the same way. C_{l6} and C_{d6} are the lift coefficients and the resistance coefficients of the whole cylinder, respectively.

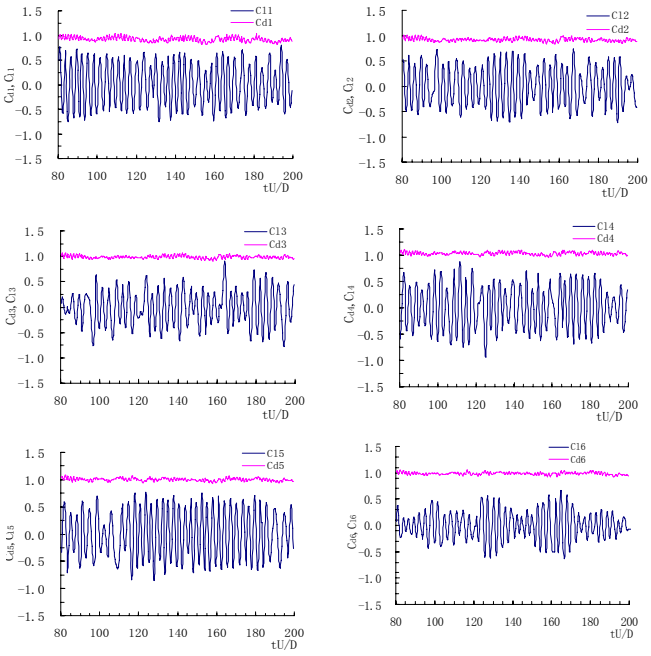

Fig.8 Duration curves of the lift coefficients and the resistance coefficients

In Fig. 8 we can see that $C_l(t)$ and $C_d(t)$ are not the same at different sections, but they are symmetrical about the middle section. The symmetry of the flow around shows that C_{l0} is 0. $C_l(t)$ is much larger than $C_d(t)$, so we can see that the effects of the lift on the cylinder are very strong, while the effects of the resistance are very weak. In Fig. 9 we can see that C_d and $C_l^{'}$ are symmetrical about the middle section, and their values are the maximum at the middle section, and then they decrease gradually toward the two ends, while the changing trend of $C_d^{'}$ is smooth.

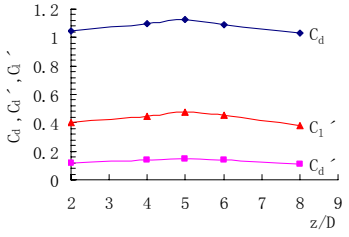

(a)

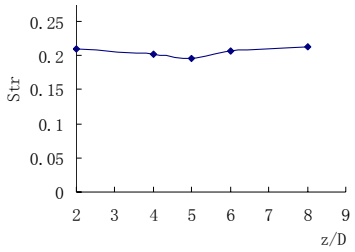

(b)

Fig. 9 Changes of C_d, C_d', C_l' and S_{tr} in the spanwise direction of the cylinder ($\mathrm{Re} = 2.2\times10^4$)

Table 1 gives the hydrodynamic parameters of the whole cylinder. By contrast in chart 1 we can see that the accuracy of the calculation on the problem of three-dimensional flow around the cylinder using the advanced turbulent model LES is higher, and the calculation error is about 5%.

Table 1 Contrast table of the hydrodynamic parameters of the cylinder

Numerical results	C_{pb}	C_{d0}	$C_d^{'}$	$C_l^{'}$
Whole cylinder	-1.108	1.072	0.132	0.429
Dong(2005)[6]	-1.129	1.143	-	0.448
Error (%)	1.9	6.2	-	4.2

From the analysis above we can see that the three-dimensional character of the flow around the cylinder is non-negligible. But the cylinder is long enough, and for each section the three-dimensional effects on the middle section is the smallest, meanwhile, in table 2 we can see that the hydrodynamic parameters of the middle section and the two-dimensional experiment results are basically identical, so we can use two-dimensional numerical method to simulate the hydrodynamic parameters of the middle section. But from chart 6 and chart 9 we can see that the hydrodynamic parameters of other sections is significantly different from those of the middle section. So the three-dimensional relativity problems must be considered when calculating the flow around the cylinder.

Table 2 Contrast table of the hydrodynamic parameters of the middle section of the three-dimensional cylinder and the two-dimensional experiment results

Numerical results	C_{pb}	$C_l^{'}$	C_{d0}
The middle section of the cylinder($z = 5D$)	-1.171	0.473	1.127
The two-dimensional cylinder experiment results[10]	-1.2	0.5	1.2
Error(%)	2.5	5.8	6.5

3.4 Stena-Haar Number

Using the lift's adaptive power spectral density function S(f) we can convert the Stena-Haar Number ($Str = \frac{f_s \times D}{u_\infty}$). The power spectral density funtions of the lift and the resistance are show in the chart below.

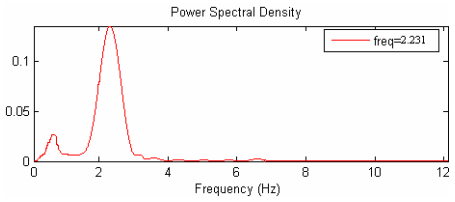

(a)

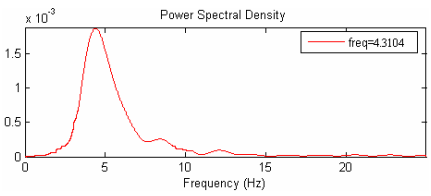

(b)

Fig. 10 the power spectral density of the lift (left) and the fluctuating resistance (right) of the section

（z=2D）

In Fig. 10 we can see that the lift changes according to the Stena-Haar frequency f_s, and the resistance consists of two parts, one part is the stable resistance not changing with time and the other part is the fluctuating resistance changing in twice the Stena-Haar frequency 2 f_s, which is consistent with the conclusions of reference [15]. S_{tr} is not obvious in the spanwise direction of the cylinder (as shown in Fig. 9), and it is symmetrical about the middle section. The contrast table of numerical results is shown in Table 3, and we can see that the advanced turbulent model LES could calculate the vortex frequency accurately when the Re number is in the sub-critical region.

Table 3 Contrast table of the calculation results of the whole cylinder's S_{tr}

S_{tr}	LES Numerical results	Pontaza [5]	Dong [6]	Gopalkrish-Nan [11]	Norberg [12]
Cylinder	0.206	0.190	0.203	0.193	0.202
Error (%)		8.4	1.5	6.73	1.98

3.5 The Form of the Vortex Shedding and the Vorticity

The form of the vortex shedding of the middle section of fluid flowing around three-dimensional cylinder is shown in Fig. 11, and the cloud picture of the pressure at each section is shown in Fig. 12.

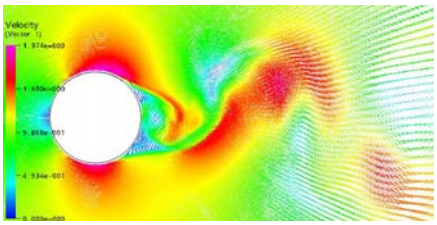

(a)

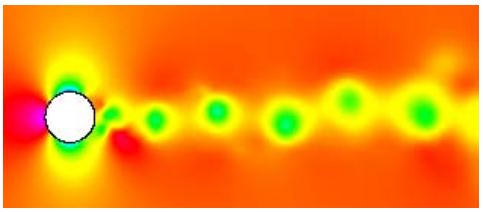

(b)

Fig.11 the cloud picture of the velocity and the pressure of the middle section

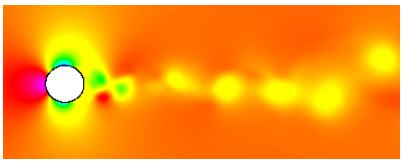

section 1

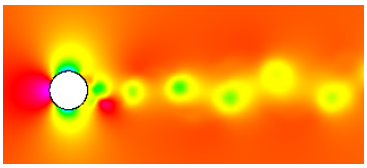

section 2

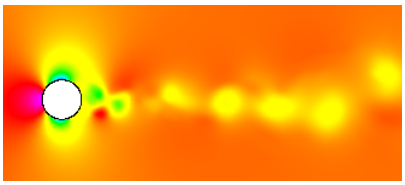

section 3

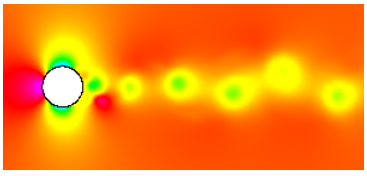

section 4

Fig. 12 Cloud picture of the pressure at each section in the spanwise direction

The three-dimensional numerical simulation of the flow around the cylinder can describe different forms of the vortex delivery in different spanwise directions. From Fig. 11 and Fig. 12 we can see that the forms of

the vortex delivery are not the same at differen xoy-sections, but it has obvious symmetry about middle section (3) in the spanwise direction. This also proves it correct that the resistance coefficients and the lift coefficients are symmetrical about the middle section.

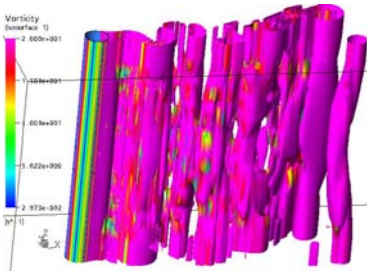

(a)

(b)

Fig. 13 Tthe vortex's iso surface (vorticity=20 m/s)

We take the vorticity Ω as the variable to draw the iso-surface of the form of the wake's vortex shedding of the three-dimensional flow around the cylinder (as shown in Fig. 13), and then we get the vortex tube describing the three-dimensional vortex delivering of the wake of the cylinder. In the spanwise direction of the cylinder, the form of the vortex shedding, the velocity and the phase of the vortex shedding and the strength of the vortex at each section are not the same, so the vortex tube is not smooth in the spanwise direction of the cylinder. This suggests that the three-dimensional character after the flow around the cylinder can not be neglected.

4. Conclusions and Prospects

By numerical experimental study of the three-dimensional flow around the cylinder, this article has mainly obtained several conclusions as follows:

(1) The stable pressure coefficients at each section in the spanwise direction of the flow around the cylinder does not change significantly, while the fluctuating pressure coefficients changes obviously.

(2) The resisitance coefficients, the lift coefficients and the Str at each section in the spanwise direction of the flow around the cylinder are symmetrical about the middle section.

(3) The vortex tube formed when the vortex of the wake of the cylinder shedding shows twisted phenomena, this suggests that the flow around the cylinder has obvious three-dimensional effects.

(4) Research will be carried out in the future: Consider the vortex delivery form and the hydrodynamic character of the three-dimensional elastic structures in the uniform flow field; use the parallel computer for many-knot numerical calculation to improve the efficiency of the numerical calculation.

Reference

[1] ZDRAVKOVICH M M. Review-review of flow interference between two circular cylinders in various arrangements [J]. Journal of Fluid Engineering, 1977:618-633p.

[2] WANG Ya-ling, LIU Ying-zhong, MIAO Guo-ping. Three-Dimensional Numerical Simulation of Viscous Flow around Circular Cylinder. JOURNAL OF SHANGHAI JIA0TONG UNIVERSITY, 2001, 35(19): 1464-1469p.

[3] Zhang Zhao-shun, Cui Gui-xiang, Xu Xiao-chun. Theory and Model of Onflow [M]. Beijing: Press of Qinghua University, 2005: 256-160p.

[4] M Breuer, A challenging test case for large eddy simulation: high Reynolds number circular cylinder flow [J] ,Heat and Fluid Flow ,2000（21）：648-654p.

[5] Juan P. Pontaza,Humn-Ching Chen,Three-dimensional numerical simulations of circular cylinders undergoing two degree-of-freedom vortex-induced vibrations [C], Proceedings of 25th international Conference on

Offshore Mechanics and Arctic Engineering, 2006: OMAE2006-92052.

[6] S. Dong, G. E. Karniadakis, DNS of flow past a stationary and oscillating cylinder at Re=10000 [J], Journal of Fluids and Structures, 2005(20): 519-531p.

[7] M.Burger, R.Schmehl,R.Koch, S.Witting, H.J.Bauer, DNS of droplet-vortex interaction with a Karman vortex street [J],Heat and Fliud Flow,2006(27): 181-191p.

[8] P. Catalano,M.Wang, G. Iaccarino, S.Witting, H.J.Bauer, Numerical simulation of the flow around a circular cylinder at high Reynolds number[J],Heat and Fliud Flow,2003(24): 463-469p.

[9] K. Lam, F. K. Wang, R. M. C. So,Three-dimensional nature of vortices in the near wake of a wavy cylinder [J], Journal of Fluids and Structures,2004(19): 815-833p.

[10] Lin Zong-hu, et al. Characteristic of the flow-fluid Shed and its Engineering Application [M]. Beijing: Press of Chemical Industry, 2001.8.

[11] R. Gopalkrishnan,Vortex-induced forces on oscillating bluff cylinder. Ph. D. Thesis,Department of Ocean Engineering, MIT, Cambridge,MA,USA,1993.

[12] C. Norberg,Fluctuating lift on a circular cylinder.review and new measurements [J], Journal of Fluids and Structures, 2003(17): 57-96p.

[13] T. Leweke, C. H. K. Williamson,Three-dimensionality instabilities in wake transition [J] ,European Journal of Mechanics B/Fluids,1998(17): 571-586p.

[14] J. Franke, W. Frank,Large eddy simulation of the flow past a circular cylinder at ReD=3900 [J], Juornal of Wind Engineering and Industrial Aerodynamics, 2002 (90): 1192-1206p.

[15] P. T. Esperanca, J. B. Wanderley, C. Levi, Validation of a three-dimensional large eddy simulation finite difference method to study vortex induced vibration[C], Proceedings of 25th international Conference on Offshore Mechanics and Arctic Engineering,2006：OMAE2006-92367p.

[16] K. Lam, F. K. Wang, R. M. C. So. Three-dimensional nature of vortices in the near wake of a wavy cylinder[J],Journal of Fluids and Structures,2004(19): 815-833p.

[17] Lu Xin-sen. Advanced Structural Dynamics [M]. Shanghai: Press of Shanghai Jiaotong University, 1992.5.

[18] CHEN Bing, LI Yu-cheng, LAI Guo-zhang. Three—dimensional calculation of oscillating flow past a circular cylinder near a plane. JOURNAl OF HYDRODYNAMICS. Ser. A, Vol.17, No. 1, Feb., 2002.

[19] CAO Feng-chan, XIANG Hal-fan. Calculation of unsteady flow around circular cylinder and a vortex induced vibration. Ser. A, Vo1.16, No. 1, Mar., 2001, 111-118p.